Analysis of Ball Rotation Behavior of Rzeppa Type Constant Velocity Joint (CVJ)

T. NAKAMURA K. ICHIKAWA H. KOBAYASHI S. SUZUKI
Y. SHINODA A. MORI Y. KIMURA Y. SUGIYAMA

The Rzeppa type constant velocity joint is widely used in the tire side of driveshafts. Analyzing joint ball rotational behavior could contribute to durability and functional improvement. To analyze ball behavior, we applied a multibody dynamics approach including a stick slip friction force model. This model allows the calculation of ball angular velocity. We have established an experiment method which quantifies ball angular velocity through multipoint measuring and graphical analysis, enabling the accurate prediction of ball behavior.

***Key Words**: rzeppa constant velocity joint, ball behavior, multibody dynamics, graphical analysis*

1. Introduction

The driveshaft (**Fig. 1**) is a part which transfers power to the tires from the engine, etc. while responding to changes in the direction the vehicle is travelling and fluctuation due to the unevenness in the road surface. Rzeppa type constant velocity joints (CVJ) are a mechanical element of the power transfer system located on the tire side of driveshafts which take the axial intersecting angle between the input axis and output axis (joint angle) and constantly transfer rotary motion. Due to the improvement in vehicle fuel efficiency and weight reduction of recent years, a demand has emerged for CVJs to also be lightweight and compact. Predicting the behavior of CVJ balls could lead to further lightening and higher functionality.

To lighten CVJs, there is a need to find a way to achieve longevity under high surface pressure but there is the difficulty of handling tribology, which deals with the dynamic contact, friction and so on of multiple parts. Moreover, due to the fact that the entire CVJ rotates, it was difficult to quantify and analyze CVJ ball behavior, as well as verify the results through experiment. As an experimental example, Nagatani and company, the authors of "Study of the BJ Ball Rotational Motion, Transactions of the JSME", have measured the rotation movement using a magnetized ball[1].

In the experiment of this study, we established a method to quantify ball behavior through arithmetic processing using the Euler Parameters concept on the rotation matrix obtained from multipoint simultaneous measurement using a high-speed camera.

Moreover, in the analysis stage, we used a model able to reproduce static friction force and dynamic friction force at a high level and built an analysis model which simulates the contact load and friction force created between parts.

This made it possible to verify the analysis results in an experiment and predict ball behavior with good accuracy. We report on the details below.

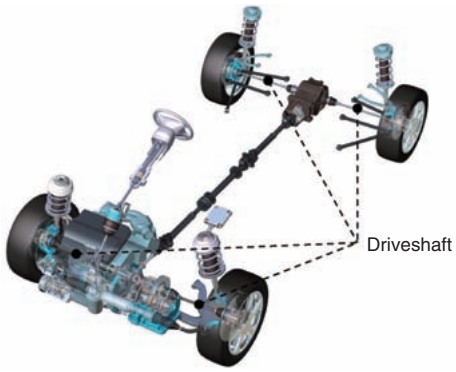

Fig. 1 Location of driveshaft on vehicle

2. Analysis Model

2. 1 Configuration of CVJ

Figure 2 shows the configuration of a CVJ. Generally speaking, CVJs are configured from an outer race, inner race, cage and six balls. The inner race is held in the inner spherical surface of the cage, while the cage is held in the inner spherical surface of the outer race. Both the outer race and inner race have six torus-shaped grooves

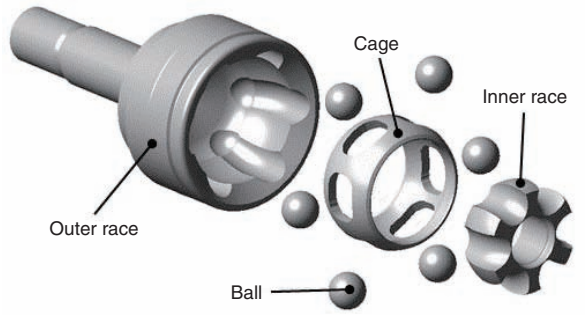

Fig. 2 Configuration of CVJ

at even intervals with each of the six balls being held in each groove and these are relatively displaced with the inner race and outer race in line with the joint angle and axial rotatory motion. The cross-sections of the grooves are a Gothic arch shape and the face which makes contact with the balls differs depending on the torque transfer direction.

2. 2 Overview of the analysis technique

Figure 3 shows the arrangement of CVJ parts at a joint angle.

For the analysis, we used general-purpose mechanism analysis software to establish an intermediate shaft, individual CVJ parts, the differential-side CVJ modeled using the contraposition which can transfer constant speed rotation on any angle and the sliding contraposition, and the testing apparatus as the rigid bodies, and arranged these on three-dimensional global coordinates.

Part of the intermediate shaft uses a beam element. Next, with contact elements alone, we correlated the outer race ball grooves, inner race ball grooves, cage window and balls, outer race inner spherical surface and cage outer spherical surface, and the cage inner spherical surface and outer spherical surface of the inner race. We connected the outer race to the outer race axis and the inner race to the intermediate shaft, and connected the outer race axis and intermediate shaft to the testing apparatus. We applied rotation, torque and joint angle from the testing apparatus and analyzed CVJ behavior.

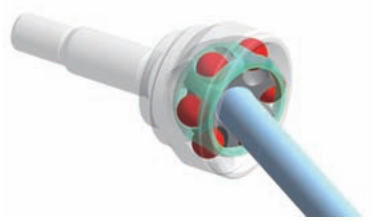

Fig. 3 Arrangement of CVJ parts at a joint angle

2. 3 Contact model

When individual surface shapes overlap, the contact load found from the penetration amount works on both contact portions. Below is the defining equation. Contact load f_n is established as the exponent of penetration amount δ expressed in the following equation and index m, coefficient C are established to suit the contact profile.

$$f_n = C\delta^m \quad (1)$$

2. 4 Friction model

2. 4. 1 Friction categories

For the friction generated within a CVJ, only the relative sliding of the contact faces of two physical objects was considered and the differential sliding, spin sliding, etc. which occurs due to the difference in the ball rotation radius of the center and edge of the ball contact ellipse, is not taken into consideration. Moreover, friction due to shearing of the grease which passes between the contact faces is also not considered.

2. 4. 2 Friction coefficient and friction force of the contact portion

Sliding friction force f_t is the sliding friction coefficient multiplied by the contact load, as expressed in the following formula.

$$f_t = \mu f_n \quad (2)$$

As shown by the bottom line of **Fig. 4**, for the conventional mechanism analysis, the friction force of the contact portion was smooth when there was relative speed from a speed of zero, however in reality, as **Fig. 5** shows, there is both static friction and dynamic friction, resulting in large error with the preconditions of analysis particularly where sliding speed is slow. Moreover, the friction coefficient is affected by surface pressure and sliding speed. “SN” in **Fig. 5** standards for “standard pressure”.

Therefore, the preconditions derived from the static friction coefficient and the dynamic friction coefficient are introduced. Each of the friction parameters were determined from a friction coefficient measurement performed in a ball-on-plate experiment.

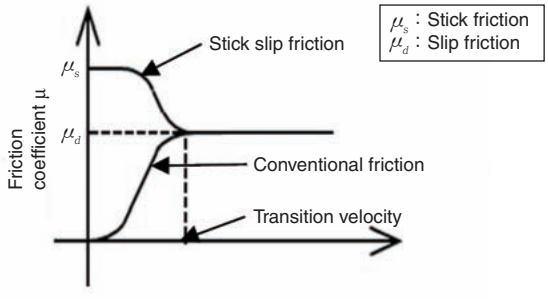

Fig. 4 Function of friction coefficient

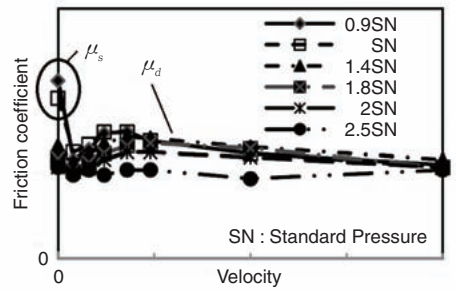

Fig. 5 Measurement results of friction coefficient from the experiment

2. 4. 3 Simulation examples of static friction and dynamic friction

Figure 7 shows an example of simulating friction force by incorporating static friction and dynamic friction on a simple ball-on-plate model (**Fig. 6**). In this way it was possible to confirm the occurrence of friction force in areas where sliding speed is slow, which conventionally could not be reproduced.

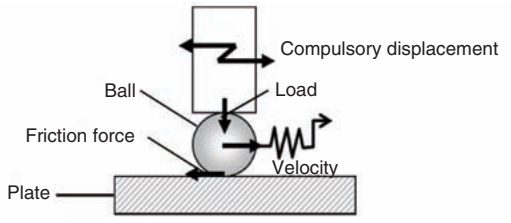

Fig. 6 Simple ball on plate model

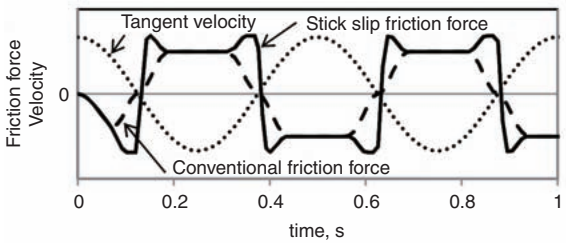

Fig. 7 Calculation results of ball on plate model

3. Analysis Results

3. 1 Analysis conditions

For analysis conditions, the same joint angle, rotating speed and torque were adopted that were used as the verification conditions in the experiment described hereinafter.

3. 2 Analysis results of ball behavior

Figure 8 shows the CVJ internal force. Moreover, each of **Fig. 9**, **10** and **11** have the CVJ rotational phase as the X axis, and respectively show the ball groove contact load, the panel angle defined as having a common contact plane for the inner race groove and ball and the outer race groove and ball, and the size of the angular velocity ω with a ball datum which only separates the rotating element.

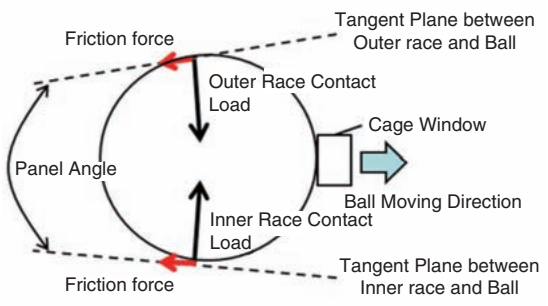

Fig. 8 CVJ internal force

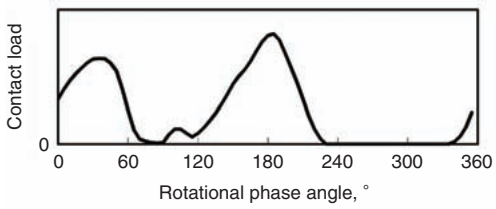

Fig. 9 Calculation results of ball contact load

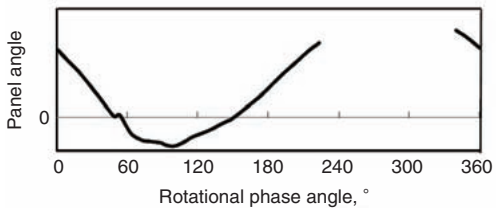

Fig. 10 Calculation results of panel angle

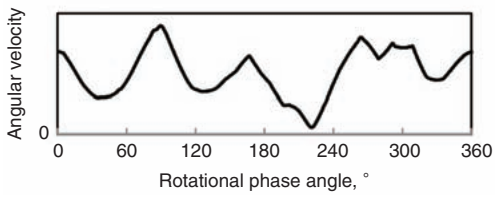

Fig. 11 Calculation results of angular velocity

4. Verification of analysis results through experiment

4. 1 Measurement and analysis method of ball rotating angular velocity

For the measurement of ball rotating motion, we devised a way to stop the ball that would normally be rotating and observe coordinates. Moreover, until now it had been impossible to observe behavior at the back of the joint however this became possible by opening a hole in the outer race.

Three points carved into the ball surface at random were simultaneously measured using a high-speed camera fixed to the outer race and graphical analysis was used to calculate the coordinates of these three points on the ball surface with the outer race as the datum.

4. 2 Calculation method of ball angular velocity

If the three arbitrary coordinates on the ball surface which use the outer race as the datum are expressed with positional vectors of $\vec{r_1}$, $\vec{r_2}$, $\vec{r_3}$ with the ball center as the starting point, the result will be as shown in **Fig. 12**. The following relationship is established between these positional vectors and angular velocity vectors.

$$\frac{d\vec{r}_i}{dt} = \vec{\omega} \times \vec{r}_i \quad (i = 1, 2, 3) \tag{3}$$

Angular velocity vectors can be obtained by solving the above simultaneous equation.

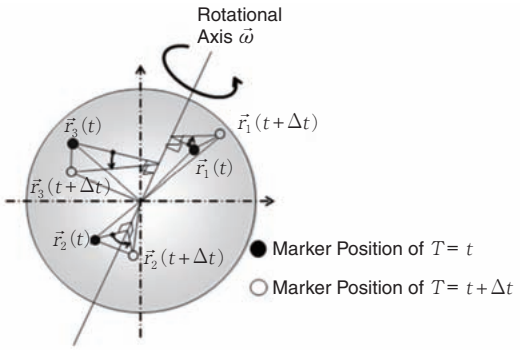

Fig. 12 Definition of ball angular velocity

Specifically, the relationship shown in Formula (5) is established between the three-dimensional coordinates which have the three ball centers as the datum in $T = T_A$ and $T = T_B$, A and B, which are expressed by a 3×3 matrix and the rotating matrix G between T_A and T_B.

$$B = GA \tag{4}$$

$$\text{Here, } A = \begin{bmatrix} x_{1A} & x_{2A} & x_{3A} \\ y_{1A} & y_{2A} & y_{3A} \\ z_{1A} & z_{2A} & z_{3A} \end{bmatrix}, B = \begin{bmatrix} x_{1B} & x_{2B} & x_{3B} \\ y_{1B} & y_{2B} & y_{3B} \\ z_{1B} & z_{2B} & z_{3B} \end{bmatrix},$$

$$G = \begin{bmatrix} g_{11} & g_{12} & g_{13} \\ g_{21} & g_{22} & g_{23} \\ g_{31} & g_{32} & g_{33} \end{bmatrix}$$

Meanwhile, if ϕ and $\lambda = [l \quad m \quad n]^T$ are made the directional vectors of the rotating angle and the rotating axis respectively and the Euler Parameter of $E_{AB} = [\varepsilon_0 \quad \varepsilon_1 \quad \varepsilon_2 \quad \varepsilon_3]^T$ as defined in Formula (5) is used to express the rotating matrix G, Formula (6) will be the case[2].

$$E_{AB} = \begin{bmatrix} \varepsilon_0 \\ \varepsilon_1 \\ \varepsilon_2 \\ \varepsilon_3 \end{bmatrix} = \begin{bmatrix} \cos\left(\frac{\phi}{2}\right) \\ l \sin\left(\frac{\phi}{2}\right) \\ m \sin\left(\frac{\phi}{2}\right) \\ n \sin\left(\frac{\phi}{2}\right) \end{bmatrix} = \begin{bmatrix} \cos\left(\frac{\phi}{2}\right) \\ \lambda \sin\left(\frac{\phi}{2}\right) \end{bmatrix} \tag{5}$$

$$G = \begin{bmatrix} \varepsilon_1^2 - \varepsilon_2^2 - \varepsilon_3^2 + \varepsilon_0^2 & 2(\varepsilon_1\varepsilon_2 - \varepsilon_3\varepsilon_0) & 2(\varepsilon_3\varepsilon_1 + \varepsilon_2\varepsilon_0) \\ 2(\varepsilon_1\varepsilon_2 + \varepsilon_3\varepsilon_0) & \varepsilon_2^2 - \varepsilon_3^2 - \varepsilon_1^2 + \varepsilon_0^2 & 2(\varepsilon_2\varepsilon_3 - \varepsilon_1\varepsilon_0) \\ 2(\varepsilon_3\varepsilon_1 - \varepsilon_2\varepsilon_0) & 2(\varepsilon_2\varepsilon_3 + \varepsilon_1\varepsilon_0) & \varepsilon_3^2 - \varepsilon_1^2 - \varepsilon_2^2 + \varepsilon_0^2 \end{bmatrix} \tag{6}$$

The angular velocity vector ω was obtained from the rotating angle ϕ which was obtained by comparing the rotating matrix G obtained from experimentation with Formula (4) with the rotating matrix G of Formula (6), the directional vector λ of the rotating axis and the time Δt between T_A and T_B.

4. 3 Results of a verification of experimental and analysis accuracy

Figures 13 and **14** show comparisons of the analysis results and experimental results. We made the rotational phase for comparison 120 to 270 degrees, as this range can be observed. As shown in **Fig. 15**, the target analysis accuracy was achieved within the rotational phase actually measured when the range from 240 degrees was excluded and if we focus on direction, the phase at which direction changes abruptly is also matching, therefore we judged there was good consistency.

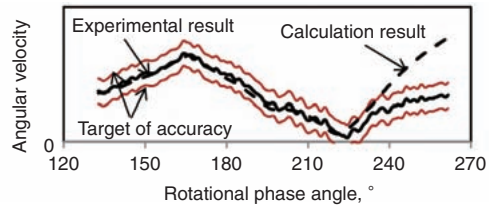

Fig. 13 Ball angular velocity comparison between calculation and actual behavior

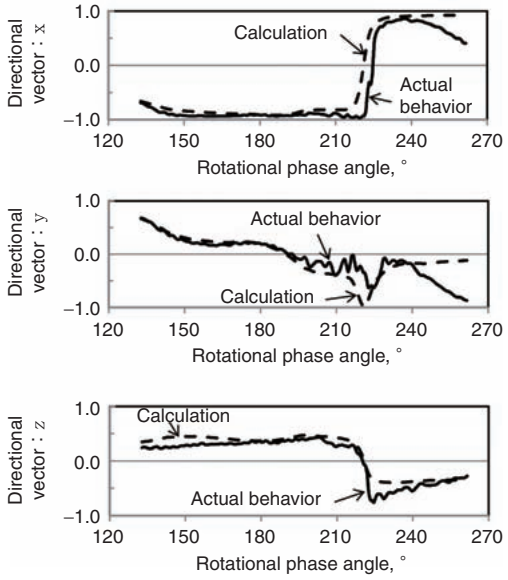

Fig. 14 Directional vector comparison between calculation and actual behavior

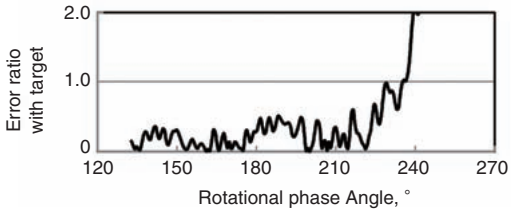

Fig. 15 Error between calculation and actual behavior

4. 4 Observations of ball behavior analysis results

During CVJ rotation, one rotation has two load peaks, as shown in **Fig. 9**, and from a rotating phase angle of 240 degrees onwards, there are phases where load dissipates. Moreover, the ball panel angle is the rotational primary period, as shown in **Fig. 10**, and determines the direction of the contact load and friction force applied to the balls.

It is believed that the ball behavior is determined by the sum of the friction force moment applied to the balls, and we predict that the analysis results reproduce contact load and its direction with good accuracy.

Meanwhile, possible factors causing error may be those other than sliding friction which are not taken into consideration as analysis preconditions, namely grease shearing friction and rolling friction. It is believed these factors have a significant impact at the phases where load dissipates.

5. Conclusion

For CVJs (Rzeppa type constant velocity joints), we quantified the ball angular velocity vectors within the CVJ on the preconditions of static friction and dynamic friction. Moreover, we performed multipoint simultaneous measurement using a high-speed camera and judged that there was accuracy in the analysis.

The establishment of this analysis method made the following items possible.

1) With conventional analysis, it was not possible to generate friction force in the portions with slow sliding speed however this has become possible by considering static friction and dynamic friction based on measurement results of friction coefficients in a ball-on-plate experiment.
2) With the preconditions of a static friction and dynamic friction model for the contact portion, it has become possible to measure CVJ ball behavior with angular speed vectors.
3) As the entire CVJ rotates, it was previously difficult to observe and quantify ball behavior, however quantification was made possible through innovative photography methods and multipoint simultaneous measurement. When compared with the analysis results, the target analysis accuracy was achieved excluding the phase range where the ball load dissipated, making it possible to predict ball behavior in theory through analysis.

This means there is a possibility of being able to predict joint durability at high accuracy and propose the optimal friction coefficient in grease development, therefore future design techniques can be expected to improve.

References

1) H. Nagatani, G. Saito, M. Imoto, S. Ishiguro: Study of the BJ Ball Rotational Motion, Transactions of the Japan Society of Mechanical Engineers, Sries C, Vol. 72, No. 716 (2006) 1249-1257
2) H. Tajima: Fundamentals of Multibody Dynamics, Tokyo Denki University Press, (2006) 77



T. NAKAMURA* K. ICHIKAWA** H. KOBAYASHI*



S. SUZUKI*** Y. SHINODA**** A. MORI****


Y. KIMURA**** Y. SUGIYAMA*****

* *Experiment & Analysis Dept., Driveline Systems Operations Headquarters*
** *Experiment & Analysis Dept., Driveline Systems Operations Headquarters, Doctor of Engineering*
*** *Driveline System Engineering Dept. 1, Driveline Systems Operations Headquarters*
**** *Drivetrain System Development & Engineering Management Div., TOYOTA MOTER CORPORATION*
***** *Material Development Div., TOYOTA MOTER CORPORATION*